Inconel 718–Copper bimetallic joints fabricated by 3D multi-material laser powder bed fusion for aerospace components

Ana Marques, Óscar Carvalho, Filipe Samuel Silva, Flávio Bartolomeu
CMEMS – Center for Microelectromechanical Systems, University of Minho, Azurém, 4800-058 Guimarães, Portugal
LABBELS – Associate Laboratory, Braga/Guimarães, Portugal

Sónia Pereira, Paulo Alexandrino
INCM – Imprensa Nacional Casa da Moeda

ABSTRACT

Usually, aerospace components are subjected to high demanding operating conditions in terms of mechanical and thermal stresses. The structural integrity of these components is assured by the use of high strength and temperature-resistant materials such as Inconel alloys. However, these alloys are known to have low thermal conductivity, which makes it difficult to extract heat from inside the component. Copper-based alloys are widely used in the aerospace field due to their high thermal conductivity, high strength, good ductility and corrosion resistance.

A 3D multi-material Inconel 718 – Copper solution was produced by laser powder bed fusion to be applied on a rocket engine wall aiming to improve its heat extraction ability. This approach combines high strength Inconel 718 and high thermal conductivity Copper in a single part, produced at once. The individual Inconel 718 and Copper zones and interface transition zone features were assessed in terms of metallurgical bonding and mechanical behaviour. This 3D multi-material Inconel 718 – Copper solution seems to be a promising approach since the two materials have a well-defined interface with no substantial defects. Inconel 718 and Copper seems to be capable to maintain its most important individual properties, high strength and high thermal conductivity.

INTRODUCTION

Additive Manufacturing (AM) processes are a group of technologies that allows to produce high quality metal parts. Material extrusion, binder or material jetting, sheet lamination, directed energy deposition (DPD) and powder bed fusion (PDF) are the most common AM processes reported in literature [1]–[3][4].

PBF technologies includes spreading of powder bed and the use a heat source to melt atomized powder particle together layer by layer until the part is completed [5]. The most common PBF technologies are Electron Beam Melting (EBM) and Laser Powder Bed Fusion (LPBF) and differ from each other in the heat source type – there are heated thermal print head, electron beam and laser, respectively [6]–[8].

LPBF technology have been reported as a promising process to obtain highly densified parts (with densification close to 100%) with satisfactory mechanical properties when compared with cast parts and close to those produced by forging. Contrarily to conventional manufacturing, this technology have a huge design freedom that allows to produce parts with complex geometries [8]–[10].

This additive manufacturing technology are deeply explored on single materials such as titanium, stainless steel or nickel alloys. However, the production of multi-material parts has several advantages over single material parts since the joining of two or more materials offers allows to benefit of a larger range of properties - such as thermal, mechanical, electrical, optical, and corrosion resistance - of the materials included [11], [12].

The development of 3D multi-material solution (material varies along the xy-axis while is built in the z-axis) by laser powder bed fusion has been rarely proposed since the powder fusion technology was first conceived. Some achievements and complications are not yet explored in 1D or 2D multi-material solutions, especially the replacing of the bed twice for each layer [16], [17]. Multi-material laser powder bed fusion technology (MMLPF) has been applied on the production of functionally graded materials (FGM) usually known as having arbitrary changes in composition to regulate final properties of a part but only presents material's changes along x-axis [13]–[15]. Significant challenges for multiple material fabrication including grading in both the vertical and horizontal directions, clearing of unwanted powder compositions from previous layers, local processing parameter changes, grading of materials with disparate melting temperature\ and demonstration of complex geometries with graded composition.

Copper alloys are usually employed in main combustion chamber in the regeneratively cooled rocket engines due to its high thermal conductivity. However, these ductile alloys are also known as having low elevated temperature strength [18]–[21]. The joining of two distinct alloys is very useful to benefit from different properties. Some works reported the production of multi-material IN718-Cu solutions through conventional manufacturing processes proved difficult, including formation of microcracks and splat boundaries. Marques et al [22] access both individual material zones and interface transition zone features in terms of metallurgical bonding and mechanical behaviour fabricated by a 3D multi-material laser powder bed fusion system. Onuike et al [23] measure shear strength of Inconel 718/copper alloy (GRCop-84) bimetallic joint built via laser engineered net shaping (LENS™). Onuike et al [24] studied the interfacial and thermal properties of Inconel 718 - GRCop-84 bimetallic structures were produced by laser engineering net shaping (LENS™).

This work presented the diffusion behaviour and interfacial characteristics of a 3D multi-material solution processed by laser powder bed fusion in which each layer is constituted by two distinct materials, Inconel 718 (IN718) and Copper (Cu). The joining of these two distinct materials is a significant challenge but also a promise in the improvement of heat extraction ability of an aerospace component. Additionally, a multi-material solution constituted by these two materials joined together can also be interesting for application in collection coins.

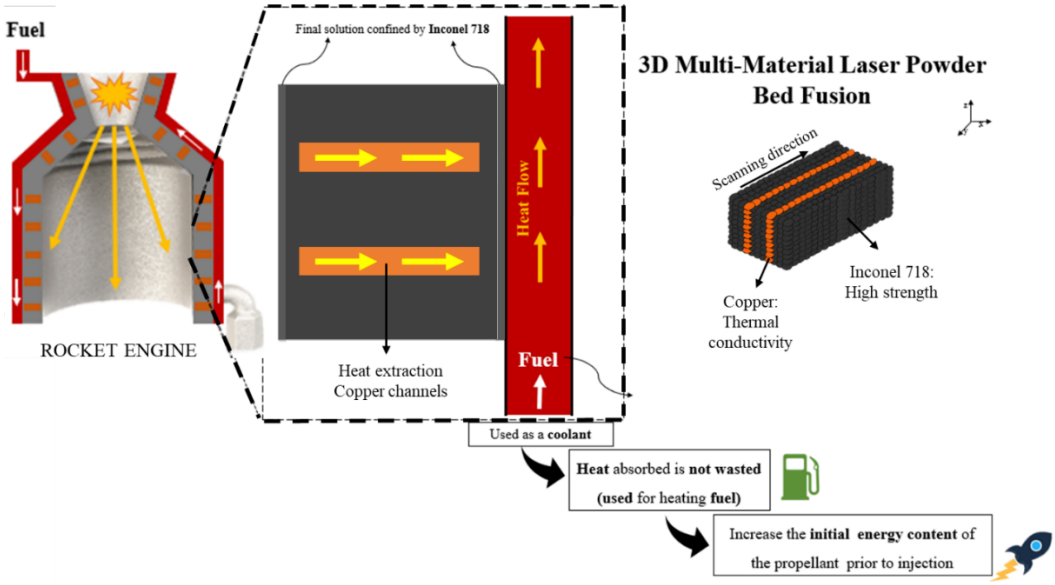

Figure 1. Design concept of the 3D multi-material IN718 – Cu solution for a rocket engine.

MATERIALS AND METHODS

Materials

IN718 and Cu powders used in this study were purchased from Carpenter Additive and TLS Technik LPW Technology suppliers, respectively, with a given particle size ranging between 15 and 45 µm. The Cu powder with 99.7% purity presented a spherical shape (Figure 2a) and IN7718 powders showed some satellites (Figure 2b).

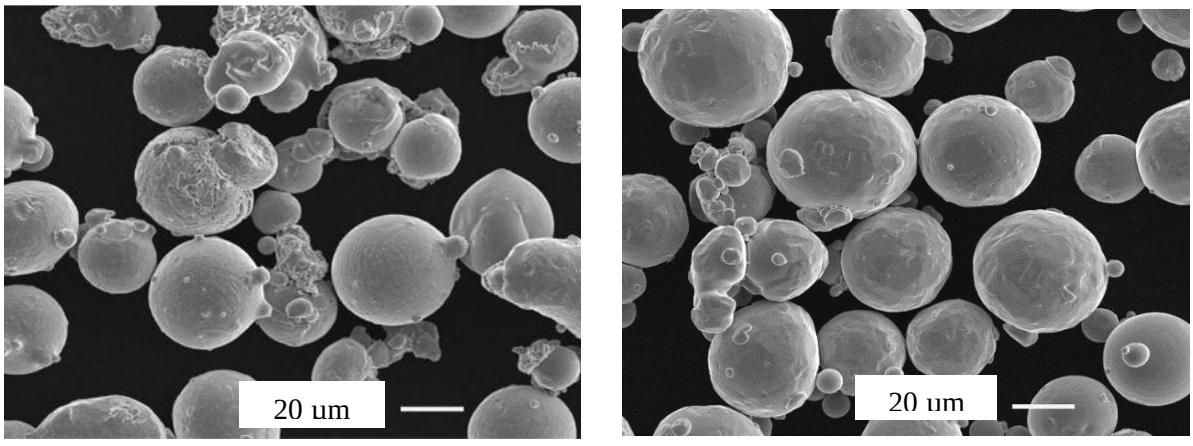

(a) (b)

Figure 2. (a) IN718 and **(b)** Cu powder's morphology.

The IN718 alloys constituted by 50.0 – 55.0 % Ni and 21.0 % Cr, 2.8 – 3.3 % that is responsible to prevent oxidation at high temperatures and of molybdenum (Mo) that avoid the pitting corrosion. This alloy have also as titanium, aluminum, cobalt and iron [25][26] (Table 1).

Table 1. Chemical composition of IN718 powder (Carpenter Additive Lda) [27].

Elements	Al	Cr	Co	Cu	Fe	Mn	Mo	Ni	Nb+Ta	Si	Ti
wt. %	0.70	21	1	0.3	Balance	0.35	2.80-3.30	50-55	4.75-5.50	0.15	1.15

Equipment

The 3D Multi-material IN718 – Cu specimens was produced using home-made Multi-Material Laser Powder Bed Fusion system (MMLPBF) developed at Center for Microelectromechanical Systems (CMEMS) at University of Minho which is equipped with an Nd: YAG laser as the heat source (maximum power of 80 W and laser wavelength (λ) of 1064 nm) represented in Figure 3a.

The 3DMMLPBF system includes two simultaneous and independent powder deposits (IN718 and Cu), two redesigned recoaters which are used to deposit two feedstock materials alternatingly and two vacuum suction systems to clean and replace the powder materials (Figure 3b). Both IN718 and Cu feedstock powders were deposited and processed on an IN718 build plate. The 3D multi-material specimens (Figure 3c) were produced under an argon atmosphere (gas pressure of 2.5 bar) in order to control the level of oxygen once this later is one of the main problem of processing copper alloys by this technology [28]. The IN718 and Cu powder were alternately deposited into the platform, allowing to fabricate 3D multi-material parts, layer-by-layer and in each layer can have different materials.

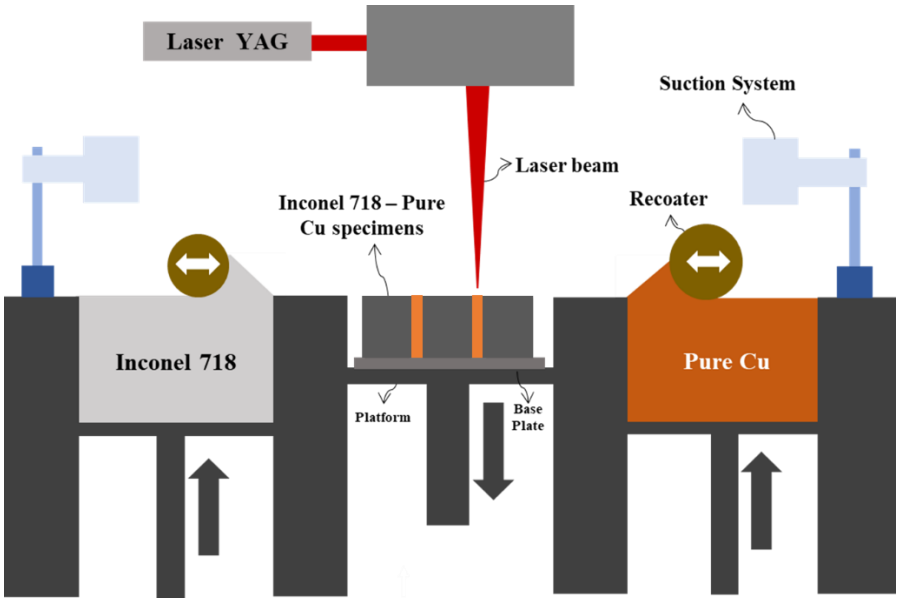

(a)

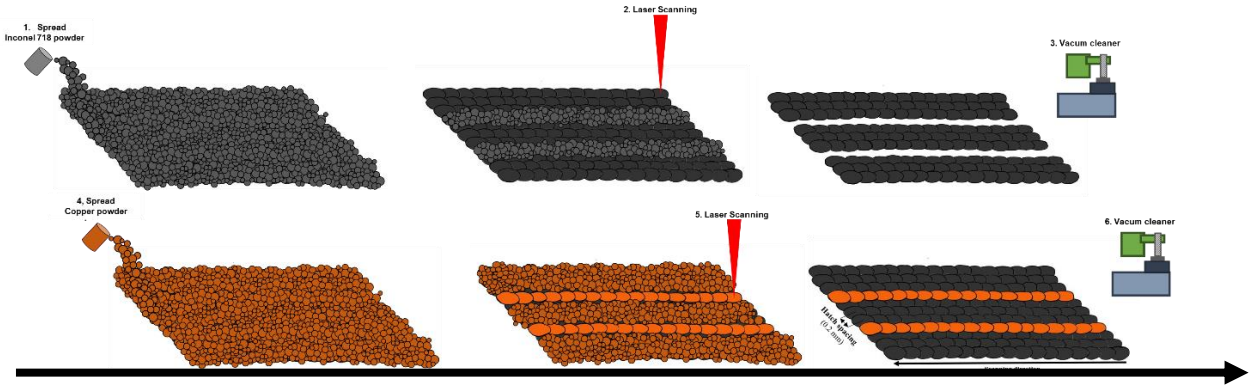

(b)

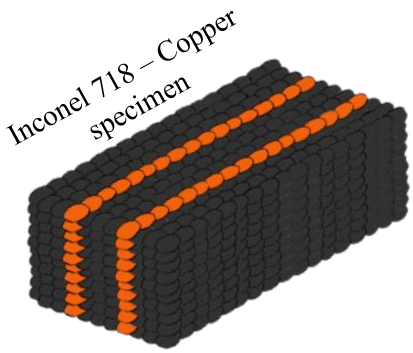

(c)

Figure 3. **(a)** Multi-Material LPBF system equipped with two powder deposits, for Inconel 718 and Pure Copper, two suctions systems and laser YAG **(b)** Main steps on the production of a single layer **(c)** Inconel 718 – Copper multi-material specimen.

The 3D multi-material specimen was designed with fifteen IN718 single scan tracks intercepted by two of Cu and each single track is separated by 200 µm (scan spacing). The processing parameters are presented Table 2. The power laser for Cu (12 W) was higher than for IN718 powder (10 W), given that the Cu has a significantly higher thermal conductivity (~400 W/mK at room temperature [29]) than IN718 (~11 W/mK) [30]. As reported by Wessel et al [12], if the processing parameters were optimized for Cu, the confined liquid melt pool temperatures of the IN718 would probably be higher than the suitable for processing.

Table 2. LPBF process parameters for the alloys and their resultant relative densities.

Processing Parameters	Inconel 718	Pure Copper
Laser Power (W)	10	10 – 15
Laser scan speed (mm/s)	120	120
Layer thickness (μm)	30	30
Hatch spacing (mm)	0.2	0.2
Remelting	No	No
Uni-directional length (mm)	4	4
Laser energy density (mm/s)	0.15	0.08 – 0.13

Characterization Techniques

Both melt pool and polished surfaces (in top and cross section sides) were analyzed through an analytical scanning electron microscope (SEM) JEOL JSM-6010LV) equipped with Electron Dispersive X-ray Spectroscopy (EDS) for further assessment of the chemical composition at the IN718, interface and Cu zones. X-ray diffraction (XRD) analysis in the interface IN718 – Cu specimens was executed by using a Bruker D8 Discover diffractometer with a classical θ-2θ analysis (Bragg-Brentano geometry utilizing CuKα radiation) in which were considered a 2θ ranging between 30 and 100º, a 4 s/step of step-time and 0.04° of step-size.

The Vickers' hardness results were assessed through a microindenter equipment from EmCoTest – DuraScan using a diamond indenter. The measurements were performed considering three load values (100, 50 and 10 g) due to ductility discrepancy between IN718 and Cu and also based on literature methodology [31], [32].

RESULTS AND DISCUSSION

Morphological characterization

Processing parameters optimization

The metallurgical bonding of IN718 and Cu in 3DMMLPBF technology was achieved through a local fusion of the powders and later consolidation (Figure 4). The IN718 processing parameters were previously optimized, and a laser power of 15 W was fixed as optimum for obtaining a consolidated IN718 part. Since literature have reported undesirable results on pure Cu solidification [33], [34], this study performed an optimization of the processing parameters for sintering Cu powder. The Cu powder was deposited and melted over the IN718 processed powder. Following this, the interface region was

melted by using the same laser power as for Cu (10, 12, 14, 14.5 and 15 W). The use of low amount of energy (10 W) proved to be insufficient to reach high densification levels of Cu. A high number of pores with irregular shapes (with tens of micrometres) were observed on top surface due to lack of fusion. The increase on the laser power to 12 W led to an increase in the number of pores found on the Cu surface, but the Cu line is still not well defined geometrically. However, when applied at 14 W laser power, the porosity was significantly reduced and the Cu line is an approximated continuous line. As the laser power, in terms of densification, seems to be close to the optimum values, the laser power was increased 0.5 W to 14, 14.5 and 15 W. The use of 15 W of laser power led a well-defined Cu continuous line without significant number of pores.

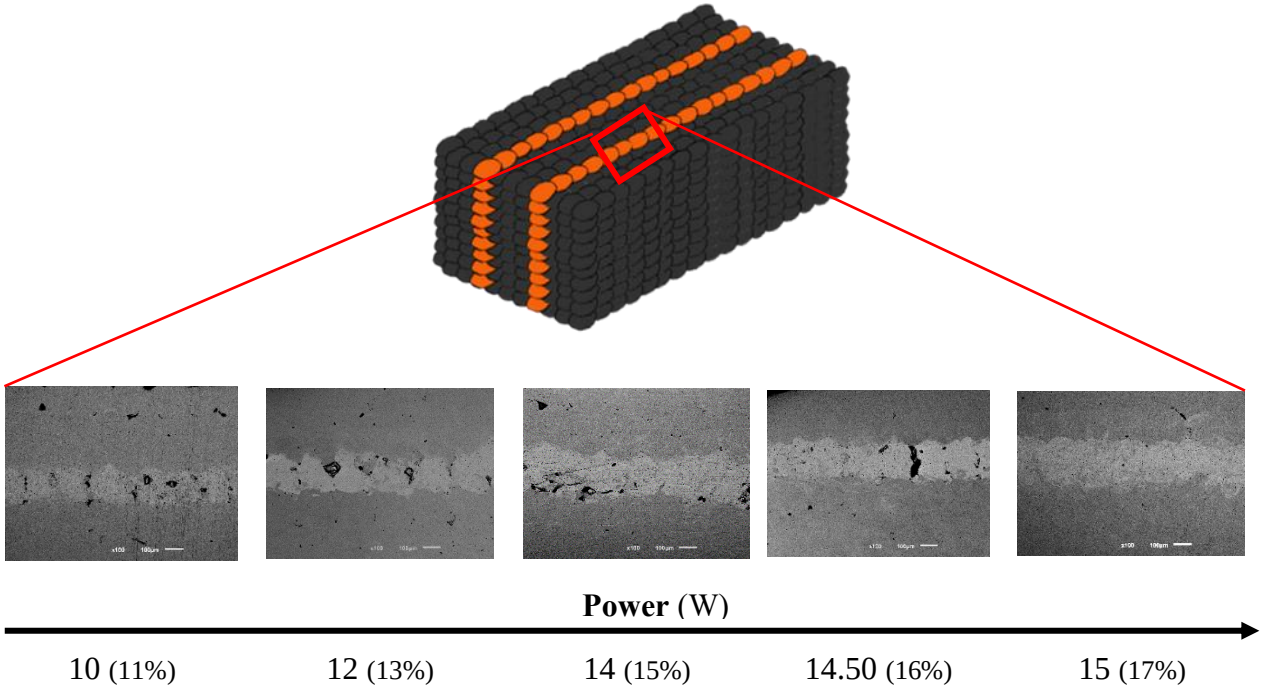

Figure 4. Top surface SEM images and EDS line across a Cu line.

The main balance on the optimization of the processing parameters for sintering Cu was to obtain a continuous and well-defined Cu line, low porosity and non-significant diffusion at the interface. It is known that the interfacial diffusion is relevant for a proper metallurgical bonding between two materials. However, the objective of this multi-material solution is to guarantee the individual properties of each material, allocated in distinct regions of the same part. In this sense, after found a laser power range (14 and 15 W) in which the Cu line are well-defined with low porosity levels, an EDS line scans from IN718 to Cu with 170 and 230 µm. Ni, Cr, Fe and Cu were the main chemical elements discussed since IN718 alloy has a limit of 0.1%wt Cu and about 50 – 55 %wt Ni [35] and the Cu, from pure Cu, having 99.7%wt Cu and 0%wt Ni. Figure 5 shows that an abrupt transition at low laser power values (12 and 14 W) and a Cu region with almost 100% of copper which means that a non-significant diffusion region are

observed at the interface. At 14.5 W, the IN718 region showed an increase on Cu element (20 – 40 %wt) and the Cu region presented some valleys coincident with peaks of Ni, Cr and Fe. The diffusion of two materials at 15 W is more evident with %wt Cu in Copper region ranging between 60 and 80 %.

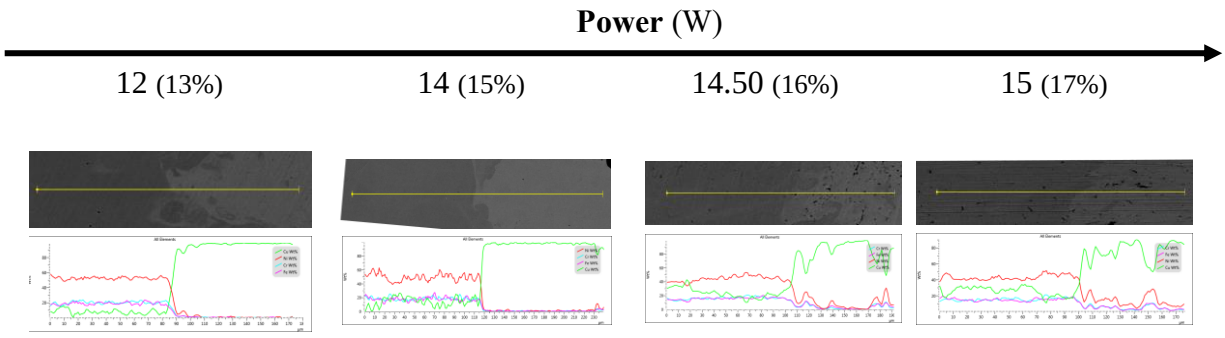

Figure 5. SEM images and EDS line across IN718 and Cu region.

Interfacial Characterization

After adjusting 3DMMLPBF processing parameters (to raise the laser energy density), the Cu powder has been reasonably solidified and bonded to the IN718 melted powder as well IN718 substrate (with a porosity of about 0.356 ± 0.05 %). Although the processing of Cu is still a challenge, the processing parameters used in the present study allowed to obtain well-defined Cu heat conductive channels with approximately 200 µm width. Residual irregular pores (with tens of micrometres) were found in Cu melted powder (as can be observed in Figure 6**Figure *6*.** Morphological characterization of the top and cross surface of the 3D multi-material IN718 – Cu specimens.) due to lack of fusion. Circular pores observed in Cu melted powder were attributed to the high cooling rate of the 3DMMLPBF technology since the gases have not time to escape, being entrapped into the solidified metal.

The Cu powder was deposited and melted over the IN718 processed powder to melt the interface region by using the laser power value of 12 W. The use of higher energy density for processing the interface leads to undergo of the IN718 processed powder and mixing with the as-deposited copper. Wits et al. [12] have reported the development of graded structures in LPBF and considered that it is advantageous to stretch the diffusion zone, creating a gradual material transition. The cracks formation also can be originated by the amount of copper at the interface during the processing process. Liu et al [36] studied the metallurgical diffusion between 316L stainless steel and C18400 copper alloy and reported that as higher the amount of copper the interface higher the possibility of creation dilute solution with iron, which strongly improves the stress at the fusion zone and so the crack formation

The IN718 inner zone is almost completely consolidated and free of defects as it is visible at the top and cross-section of the SEM images (Figure 4). Some occasionally circular shaped pores are still perceptible, which may have originated by gas entrapping during the processing [37]. These results

allowed us to conclude that the applied laser energy density was enough to melt the IN718 material, without lack of fusion.

The use of high energy the processing parameters used in the present study allowed to obtain well-defined Cu heat conductive channels with approximately 200 µm width. Circular pores observed in Cu melted powder were attributed to the high cooling rate of the 3DMMLPBF technology since the gases have not time to escape, being entrapped into the solidified metal.

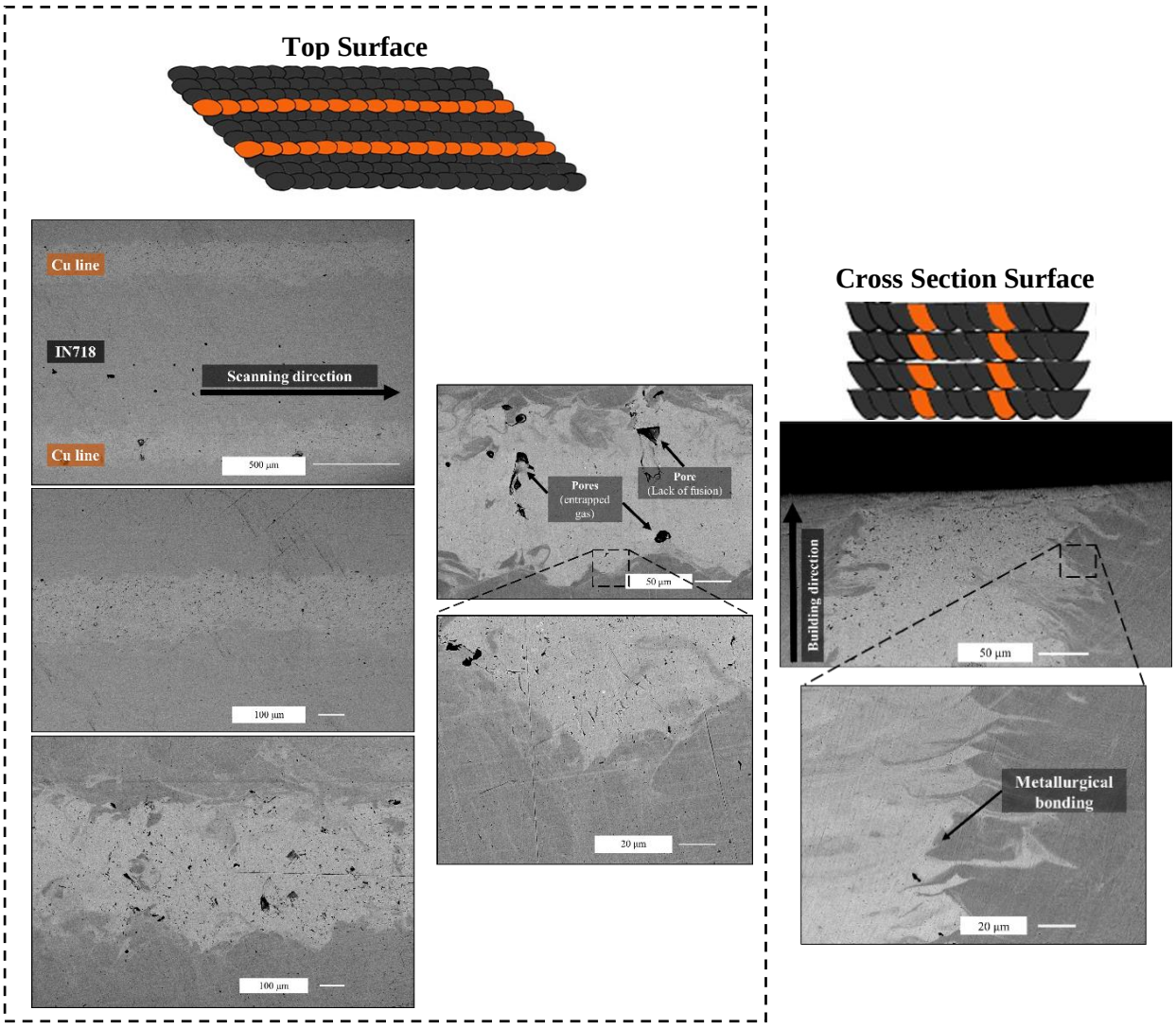

Figure 6. Morphological characterization of the top and cross surface of the 3D multi-material IN718 – Cu specimens.

EDS elemental spectra of Ni, Fe and Cr (main chemical elements of IN718) and Cu are shown in **Error! Reference source not found.**. The IN718 is mainly made of Ni (represented in red), with approximately 50 - 60 % and the Cu zone wt.% is quite high ranging from 80 to 100 (represented in orange). The interface region is represented by a gradual transition between IN718 and Cu with a significant amount of Ni and Cu element diffusion (about 25 µm thickness) at the interface region suggested a metallurgical bonding (confirmed in). Small jumps in Ni and Cu detection can be observed at 25 µm and 75 µm

distance, suggesting that there is an insignificant intermixed powders zone close to the interface may due to an incomplete suction of the powders.

These results indicate strong evidence that this new 3DMMLPBF concept is successful mainly due the presence of a well processed Cu line. The high cooling right of the this technology indicate a fast solidification, avoiding the generation of large diffusion areas in the interface zones and thus, preventing the existence of fragile zones and undesirable intermetallic phases, as reported elsewhere [13].

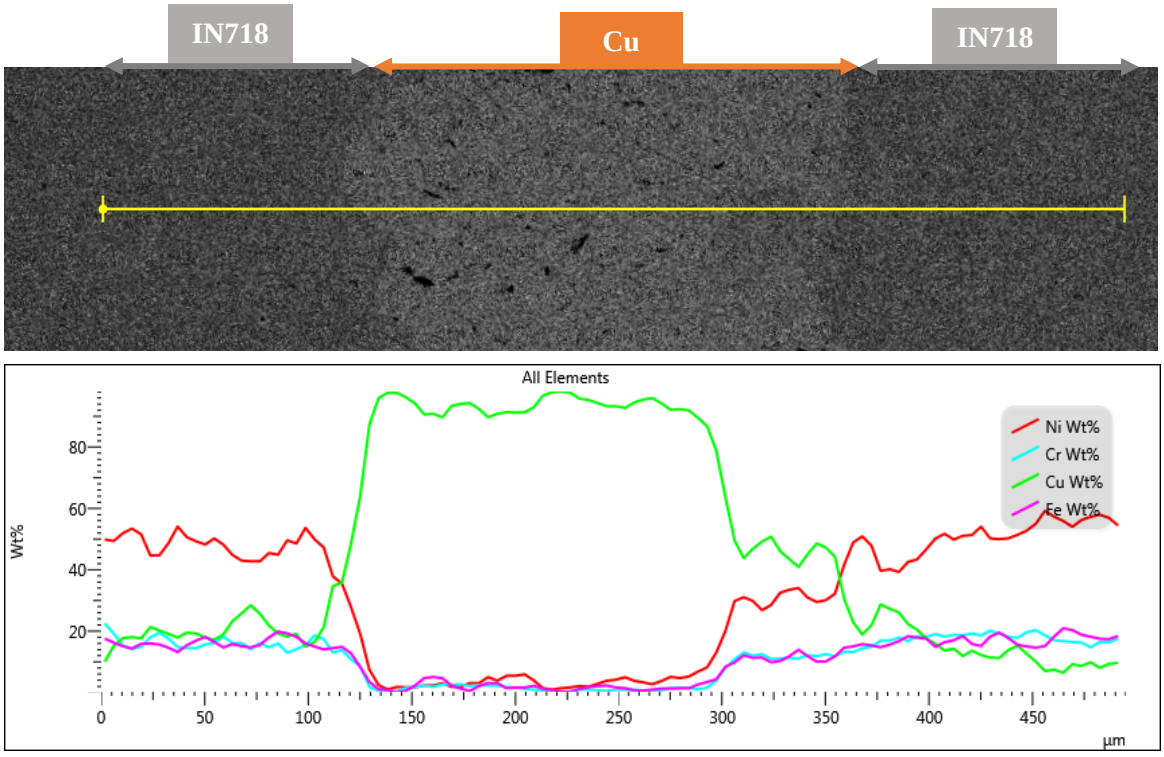

Figure 7. EDS mapping line crossing IN718, interface and Cu zones.

The XRD pattern is coincidental to the solid solution of austenite (γ) constituted by a single phased structure with Ni and Fe (the most important elements of IN718) [38]. Figure 8 showed the XRD patterns at the interface IN718 – Cu with peaks of IN718 and Cu at different angles of diffraction that are overlaid with each other. This indicate that only a single-phase solid-solution were formatted at the interface as can be confirmed in the binary equilibrium phase diagram Ni – Cu. Therefore, the absence of two-phase solid solution is beneficial since it avoids the formation of brittle intermetallic at the interface. On the other hand, the formation of a single phase at the interface induces a suitable metallurgical bonding as well high strength at the interface.

There should be underlined that the alignment of XRD peaks from different materials (IN718 and Cu), observed in Figure 8, indicate the interfacial zone carried the features of both IN718 and Cu single-phase solid solutions.

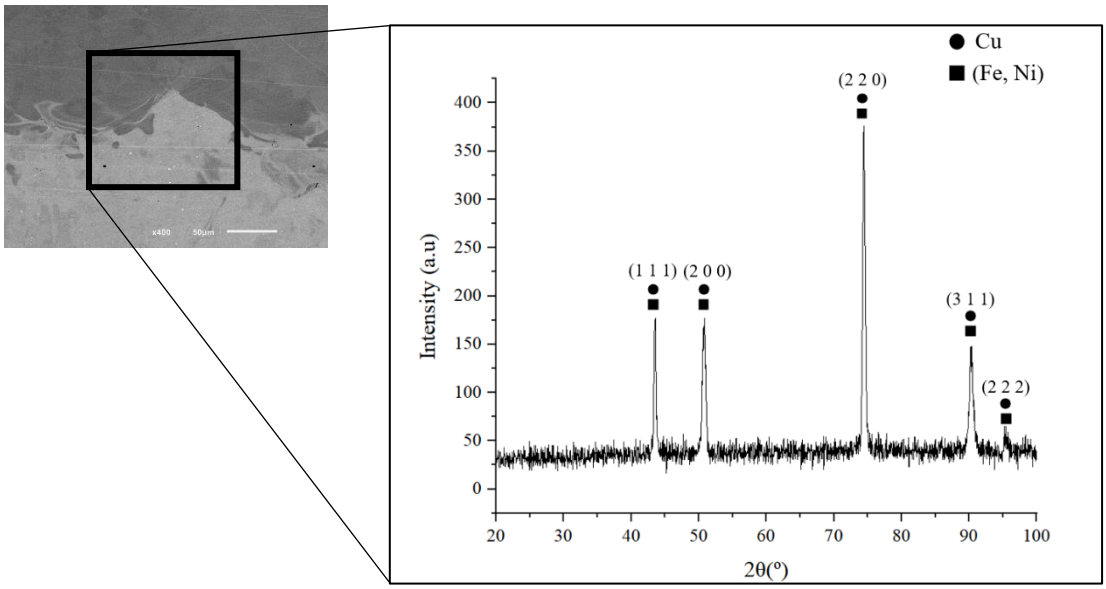

Figure 8. XRD analysis across IN718 – Cu interface.

It is known that performing hardness tests can provide relevant inputs regarding the plastic deformation of a material. Moreover, the resistance to wear (by friction or erosion by steam, oil or water) of aerospace components under harsh environments can also be indicted by hardness results [39].

Hardness Characterization

Vickers' microhardness was measured considering three load values (100, 50 and 10 g) since the two materials exhibit a very different ductility. Moreover, these measurements were taken in the left, middle and right side of the specimen in order to study how the strategy influences the hardness results along the specimen (see Figure 9). Regarding IN718 zone, the hardness measurements considered a load of 100 and 50 g and the results proved that there was no significant hardness discrepancy between distinct regions. Moreover, the hardness range values (from 292 ± 11 to 344 ± 12 HV) are coherent with those reported in literature concerning the as-built LPBFed IN718 specimens (275 - 350 HV) [40]–[63]. In agreement with the multi-material IN718 – Cu solution chemical composition (which transit from 100% IN718 to almost 100% Cu), the hardness values jumped from 344 to 126 HV respectively.

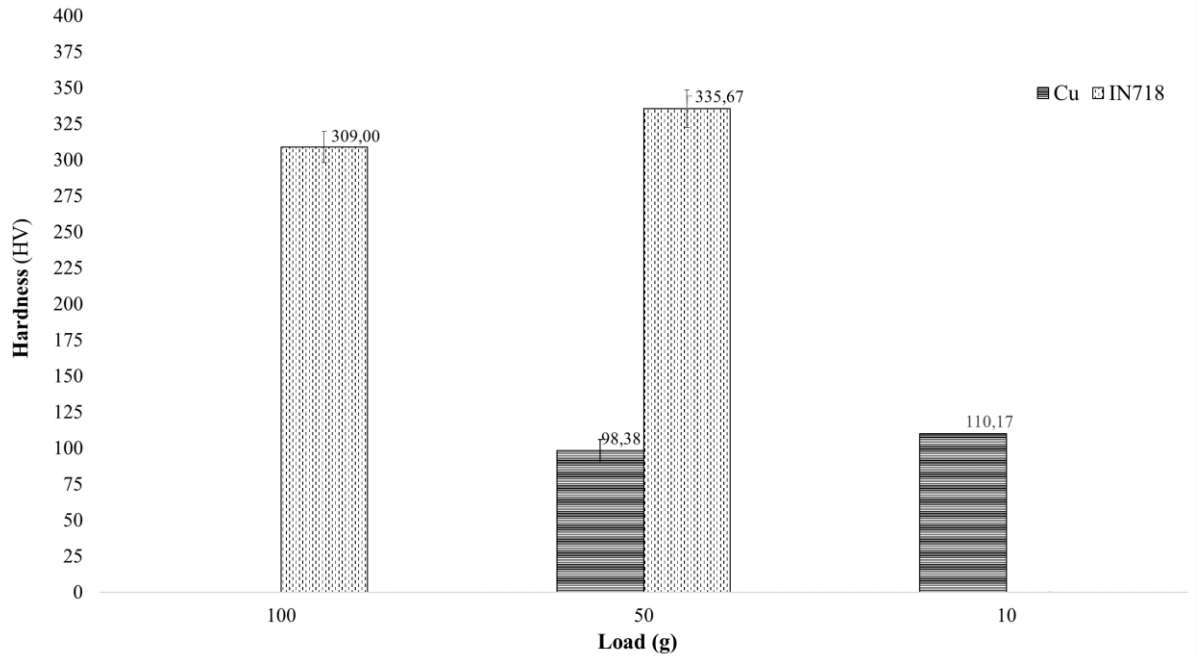

Figure 9. Vickers's microhardness results considering 100, 50 and 10 g at IN718 and Cu zones.

CONCLUSIONS

This first approach on producing 3D multi-material IN718 - Cu specimens by Laser Powder Bed Fusion here presented was considered successful. The IN718 zones are almost free of defects and show hardness values ranging the values reported in literature. On the other hand, the Cu lines present a well-defined geometry with about 200 µm width and occasional defects. A thin diffusion zone of about 25 µm is present in the transition between IN718 and Cu. In this sense, the samples produced by this new 3DMMLPBF system presented a metallurgical bonding at the most critical zone (interface) as well as a desirable metallurgical bonding between these two distinct materials. Also, there are no evidence of the formation of intermetallic compounds. This is the first work indicating the hardness values for Cu powder processed by LPBF (~126 HV). Future works should focus on studying the metallurgical features, mechanical and thermal analysis under rocket engines operation conditions.

FUNDING RESOURCES

This work was supported by FCT national funds, under the national support to R&D units grant, through the reference projects SFRH/BD/148031/2019, UIDB/04436/2020 and UIDP/04436/2020. Also, the project Add: additive - add additive manufacturing to Portuguese industry [grant number POCI-01-0247-FEDER-024533]. Additionally, this work was supported by the project Moedinov - New aesthetics for collection coins by using advanced technologies with the reference POCI-01-0247-FEDER-033361.

BIBLIOGRAPHY

[1] S. Rouf, A. Malik, N. Singh, A. Raina, N. Naveed, M. I. H. Siddiqui, and M. I. U. Haq, "Additive manufacturing technologies: Industrial and medical applications," *Sustain. Oper. Comput.*, vol. 3, no. January, pp. 258–274, 2022, doi: 10.1016/j.susoc.2022.05.001.

[2] F. J. Mercado Rivera and A. J. Rojas Arciniegas, "Additive manufacturing methods: techniques, materials, and closed-loop control applications," *Int. J. Adv. Manuf. Technol.*, vol. 109, no. 1–2, pp. 17–31, 2020, doi: 10.1007/s00170-020-05663-6.

[3] A. Vafadar, F. Guzzomi, A. Rassau, and K. Hayward, "Advances in Metal Additive Manufacturing : A Review of Common Processes , Industrial Applications , and Current Challenges," 2021.

[4] A. Pajonk, A. Prieto, U. Blum, and U. Knaack, "Multi-material additive manufacturing in architecture and construction: A review," *J. Build. Eng.*, vol. 45, no. November 2021, p. 103603, 2022, doi: 10.1016/j.jobe.2021.103603.

[5] M. Leary, "Chapter 11 - Powder bed fusion," in *Design for Additive Manufacturing, Additive Manufacturing Materials and Technologies*, 2020, pp. 295–319. doi: https://doi.org/10.1016/B978-0-12-816721-2.00011-7.

[6] S. H. Sun, Y. Koizumi, T. Saito, K. Yamanaka, Y. P. Li, Y. Cui, and A. Chiba, "Electron beam additive manufacturing of Inconel 718 alloy rods: Impact of build direction on microstructure and high-temperature tensile properties," *Addit. Manuf.*, vol. 23, no. July 2017, pp. 457–470, 2018, doi: 10.1016/j.addma.2018.08.017.

[7] A. R. Balachandramurthi, J. Moverare, S. Mahade, and R. Pederson, "Additive manufacturing of alloy 718 via electron beam melting: Effect of post-treatment on the microstructure and the mechanical properties," *Materials (Basel).*, vol. 12, no. 1, 2018, doi: 10.3390/ma12010068.

[8] A. Marques, Â. Cunha, M. R. Silva, M. I. Osendi, F. S. Silva, Ó. Carvalho, and F. Bartolomeu, "Inconel 718 produced by laser powder bed fusion: an overview of the influence of processing parameters on microstructural and mechanical properties," *Int. J. Adv. Manuf. Technol.*, vol. 121, no. 9–10, pp. 5651–5675, 2022, doi: 10.1007/s00170-022-09693-0.

[9] N. Alloy, Z. Tian, C. Zhang, D. Wang, W. Liu, and X. Fang, "A Review on Laser Powder Bed Fusion of Inconel 625," *Appl. Scien*, 2020.

[10] J. Elambasseril, J. Rogers, C. Wallbrink, D. Munk, M. Leary, and M. Qian, "Laser powder bed fusion additive manufacturing (LPBF-AM): the influence of design features and LPBF

variables on surface topography and effect on fatigue properties," *Crit. Rev. Solid State Mater. Sci.*, vol. 0, no. 0, pp. 1–37, 2022, doi: 10.1080/10408436.2022.2041396.

[11] D. Wang, L. Liu, G. Deng, C. Deng, Y. Bai, Y. Yang, W. Wu, J. Chen, Y. Liu, Y. Wang, X. Lin, and C. Han, "Recent progress on additive manufacturing of multi-material structures with laser powder bed fusion," *Virtual Phys. Prototyp.*, vol. 17, no. 2, pp. 329–365, 2022, doi: 10.1080/17452759.2022.2028343.

[12] W. W. Wits and E. Amsterdam, "Graded structures by multi-material mixing in laser powder bed fusion," *CIRP Ann.*, vol. 70, no. 1, pp. 159–162, 2021, doi: 10.1016/j.cirp.2021.03.005.

[13] M. Naebe and K. Shirvanimoghaddam, "Functionally graded materials: A review of fabrication and properties," *Appl. Mater. Today*, vol. 5, pp. 223–245, 2016, doi: 10.1016/j.apmt.2016.10.001.

[14] B. E. Carroll, R. A. Otis, J. P. Borgonia, J. O. Suh, R. P. Dillon, A. A. Shapiro, D. C. Hofmann, Z. K. Liu, and A. M. Beese, "Functionally graded material of 304L stainless steel and inconel 625 fabricated by directed energy deposition: Characterization and thermodynamic modeling," *Acta Mater.*, vol. 108, pp. 46–54, 2016, doi: 10.1016/j.actamat.2016.02.019.

[15] V. A. Popovich, E. V. Borisov, A. A. Popovich, V. S. Sufiiarov, D. V. Masaylo, and L. Alzina, "Functionally graded Inconel 718 processed by additive manufacturing: Crystallographic texture, anisotropy of microstructure and mechanical properties," *Mater. Des.*, vol. 114, pp. 441–449, 2017, doi: 10.1016/j.matdes.2016.10.075.

[16] S. Hasanov, S. Alkunte, M. Rajeshirke, A. Gupta, O. Huseynov, I. Fidan, F. Alifui-Segbaya, and A. Rennie, "Review on additive manufacturing of multi-material parts: Progress and challenges," *J. Manuf. Mater. Process.*, vol. 6, no. 1, 2022, doi: 10.3390/jmmp6010004.

[17] C. Wei and L. Li, "Recent progress and scientific challenges in multi-material additive manufacturing via laser-based powder bed fusion," *Virtual Phys. Prototyp.*, vol. 16, no. 3, pp. 347–371, 2021, doi: 10.1080/17452759.2021.1928520.

[18] K. C. Bendall, "Copper alloys for critical aircraft and aerospace components," 1995. https://www.emerald.com/insight/content/doi/10.1108/eb037566/full/html?skipTracking=true

[19] D. Soares, D. Almeida, W. Shimote, A. Wilson, K. Shimote, and M. Niwa, "Selection of Materials for Combustion Chamber of Liquid Propellant Rocket Engine," no. November, 1999.

[20] J. Singh, "Fabrication of High Thermal Conductivity NARloy-Z-Diamond Composite Combustion Chamber Liner for Advanced Rocket Engines," *NASA- Marshall Sp. Flight Center, Pennsylvania*.

[21] W. Emrich, *Rocket Engine Fundamentals*. Huntsville, USA, 2016. doi: 10.1016/b978-0-12-804474-2.00002-3.

[22] A. Marques, Â. Cunha, M. Gasik, O. Carvalho, F. S. Silva, and F. Bartolomeu, "Inconel 718–copper parts fabricated by 3D multi-material laser powder bed fusion: a novel technological and designing approach for rocket engine," *Int. J. Adv. Manuf. Technol.*, vol. 122, no. 3–4, pp. 2113–2123, 2022, doi: 10.1007/s00170-022-10011-x.

[23] B. Onuike and A. Bandyopadhyay, "Bond strength measurement for additively manufactured Inconel 718- GRCop84 copper alloy bimetallic joints," *Addit. Manuf.*, vol. 27, no. April, pp. 576–585, 2019, doi: 10.1016/j.addma.2019.04.003.

[24] B. Onuike, B. Heer, and A. Bandyopadhyay, "Additive manufacturing of Inconel 718—Copper alloy bimetallic structure using laser engineered net shaping (LENS^{TM})," *Addit. Manuf.*, vol. 21, no. February, pp. 133–140, 2018, doi: 10.1016/j.addma.2018.02.007.

[25] H. Y. Ha, T. H. Lee, J. H. Bae, and D. W. Chun, "Molybdenum effects on pitting corrosion resistance of FeCrMnMoNC austenitic stainless steels," *Metals (Basel).*, vol. 8, no. 8, pp. 1–13, 2018, doi: 10.3390/met8080653.

[26] J. H. Suwardie, R. Artiaga, and J. L. Mier, "Thermal characterization of a Ni-based superalloy," *Thermochim. Acta*, vol. 392–393, pp. 295–298, 2002, doi: 10.1016/S0040-6031(02)00112-0.

[27] A. Manufacturing, C. Additive, C. Additive, C. T. Powderrange, S. Steel, C. T. Powderrange, L. Powder, B. Fusion, and C. T. Powderrange, "TECHNICAL DATA SHEET CT PowderRange 316L F," *Carpenter Additive Technical Data sheets*, 2019.

[28] H. Hao, Y. Wang, H. R. J. Nodooshan, Y. Zhang, S. Ye, Y. Lv, and P. Yu, "The effects of sintering temperature and addition of TiH2 on the sintering process of Cu," *Materials (Basel).*, vol. 12, no. 16, 2019, doi: 10.3390/ma12162594.

[29] "Copper propertiess," *Matweb*. http://matweb.com/search/DataSheet.aspx?MatGUID=9aebe83845c04c1db5126fada6f76f7e&ckck=1 (accessed Jan. 17, 2022).

[30] "Inconel 718 alloy," *Matweb*. http://www.matweb.com/search/datasheet.aspx?matguid=94950a2d209040a09b89952d45086134 (accessed Feb. 22, 2022).

[31] C. A. Huang, T. H. Wang, C. H. Lee, and W. C. Han, "A study of the heat-affected zone (HAZ) of an Inconel 718 sheet welded with electron-beam welding (EBW)," *Mater. Sci. Eng. A*, vol. 398, no. 1–2, pp. 275–281, 2005, doi: 10.1016/j.msea.2005.03.029.

[32] N. Ergin, O. Ozdemir, S. Demirkiran, S. Sen, and U. Sen, “Synthesis of inconel 718 superalloy by electric current activated sintering,” *Acta Phys. Pol. A*, vol. 127, no. 4, pp. 1100–1102, 2015, doi: 10.12693/APhysPolA.127.1100.

[33] M. Colopi, A. G. Demir, L. Caprio, and B. Previtali, “Limits and solutions in processing pure Cu via selective laser melting using a high-power single-mode fiber laser,” *Int. J. Adv. Manuf. Technol.*, vol. 104, no. 5–8, pp. 2473–2486, 2019, doi: 10.1007/s00170-019-04015-3.

[34] L. Bertoldo Benedetti, C. A. Comelli, and C. Ahrens, “Study on Selective Laser Melting of Copper,” no. January, 2017, doi: 10.26678/abcm.cobef2017.cof2017-0148.

[35] S. Metals, “INCONEL 718 alloy,” 2007. www.specialmetals.com (accessed Mar. 20, 2021).

[36] Z. H. Liu, D. Q. Zhang, S. L. Sing, C. K. Chua, and L. E. Loh, “Interfacial characterization of SLM parts in multi-material processing: Metallurgical diffusion between 316L stainless steel and C18400 copper alloy,” *Mater. Charact.*, vol. 94, pp. 116–125, 2014, doi: 10.1016/j.matchar.2014.05.001.

[37] R. Ding, J. Yao, B. Du, K. Li, T. Li, L. Zhao, and Y. Guo, “Effect of shielding gas volume flow on the consistency of microstructure and tensile properties of 316l manufactured by selective laser melting,” *Metals (Basel).*, vol. 11, no. 2, pp. 1–14, 2021, doi: 10.3390/met11020205.

[38] M. C. Chaturvedi and Y. Han, “Strengthening mechanisms in Inconel 718 superalloy,” *Met. Sci.*, vol. 17, no. March, pp. 145–149, 1983, doi: https://doi.org/10.1179/030634583790421032.

[39] “Materials and Hardness Testing - The Importance of its Applications,” *AZO, materials*, 2018. https://www.azom.com/article.aspx?ArticleID=15122 (accessed Feb. 11, 2022).

[40] Q. Jia and D. Gu, “Selective laser melting additive manufacturing of Inconel 718 superalloy parts: Densification, microstructure and properties,” *J. Alloys Compd.*, vol. 585, pp. 713–721, 2014, doi: 10.1016/j.jallcom.2013.09.171.

[41] Q. B. Nguyen, D. N. Luu, S. M. L. Nai, Z. Zhu, Z. Chen, and J. Wei, “The role of powder layer thickness on the quality of SLM printed parts,” *Arch. Civ. Mech. Eng.*, vol. 18, no. 3, pp. 948–955, 2018, doi: 10.1016/j.acme.2018.01.015.

[42] D. A. Lesyk, S. Martinez, B. N. Mordyuk, V. V. Dzhemelinskyi, Lamikiz, and G. I. Prokopenko, “Post-processing of the Inconel 718 alloy parts fabricated by selective laser melting: Effects of mechanical surface treatments on surface topography, porosity, hardness and residual stress,” *Surf. Coatings Technol.*, vol. 381, no. October 2019, p. 125136, 2020, doi: 10.1016/j.surfcoat.2019.125136.

[43] X. Li, J. J. Shi, C. H. Wang, G. H. Cao, A. M. Russell, Z. J. Zhou, C. P. Li, and G. F. Chen, "Effect of heat treatment on microstructure evolution of Inconel 718 alloy fabricated by selective laser melting," *J. Alloys Compd.*, vol. 764, pp. 639–649, 2018, doi: 10.1016/j.jallcom.2018.06.112.

[44] R. Jiang, A. Mostafaei, J. Pauza, C. Kantzos, and A. D. Rollett, "Varied heat treatments and properties of laser powder bed printed Inconel 718," *Mater. Sci. Eng. A*, vol. 755, no. March, pp. 170–180, 2019, doi: 10.1016/j.msea.2019.03.103.

[45] R. Jiang, A. Mostafaei, Z. Wu, A. Choi, P. W. Guan, M. Chmielus, and A. D. Rollett, "Effect of heat treatment on microstructural evolution and hardness homogeneity in laser powder bed fusion of alloy 718," *Addit. Manuf.*, vol. 35, no. April, p. 101282, 2020, doi: 10.1016/j.addma.2020.101282.

[46] H. Song, T. McGaughy, A. Sadek, and W. Zhang, "Effect of structural support on microstructure of nickel base superalloy fabricated by laser-powder bed fusion additive manufacturing," *Addit. Manuf.*, vol. 26, no. December 2018, pp. 30–40, 2019, doi: 10.1016/j.addma.2018.12.017.

[47] C. Samuel. S, M. Arivarasu, and T. R. Prabhu, "High temperature dry sliding wear behaviour of laser powder bed fused Inconel 718," *Addit. Manuf.*, vol. 34, no. April, p. 101279, 2020, doi: 10.1016/j.addma.2020.101279.

[48] E. Park, D. M. Kim, H. W. Park, Y. Bin Park, and N. Kim, "Evaluation of Tool Life in the Dry Machining of Inconel 718 Parts from Additive Manufacturing (AM)," *Int. J. Precis. Eng. Manuf.*, vol. 21, no. 1, pp. 57–65, 2020, doi: 10.1007/s12541-019-00275-x.

[49] Y. Lu, S. Wu, Y. Gan, T. Huang, C. Yang, L. Junjie, and J. Lin, "Study on the microstructure, mechanical property and residual stress of SLM Inconel-718 alloy manufactured by differing island scanning strategy," *Opt. Laser Technol.*, vol. 75, pp. 197–206, 2015, doi: 10.1016/j.optlastec.2015.07.009.

[50] D. J. Newell, R. P. O'Hara, G. R. Cobb, A. N. Palazotto, M. M. Kirka, L. W. Burggraf, and J. A. Hess, "Mitigation of scan strategy effects and material anisotropy through supersolvus annealing in LPBF IN718," *Mater. Sci. Eng. A*, vol. 764, no. August, p. 138230, 2019, doi: 10.1016/j.msea.2019.138230.

[51] Y. Cao, P. Bai, F. Liu, X. Hou, and Y. Guo, "Effect of the solution temperature on the precipitates and grain evolution of IN718 fabricated by laser additive manufacturing," *Materials (Basel).*, vol. 13, no. 2, 2020, doi: 10.3390/ma13020340.

[52] F. Caiazzo, V. Alfieri, and G. Casalino, "On the Relevance of volumetric energy density in the investigation of inconel 718 laser powder bed fusion," *Materials (Basel).*, vol. 13, no. 3, pp. 1–

12, 2020, doi: 10.3390/ma13030538.

[53] Z. Wang, K. Guan, M. Gao, X. Li, X. Chen, and X. Zeng, “The microstructure and mechanical properties of deposited-IN718 by selective laser melting,” *J. Alloys Compd.*, vol. 513, pp. 518–523, 2012, doi: 10.1016/j.jallcom.2011.10.107.

[54] E. Chlebus, K. Gruber, B. Kuźnicka, J. Kurzac, and T. Kurzynowski, “Effect of heat treatment on the microstructure and mechanical properties of Inconel 718 processed by selective laser melting,” *Mater. Sci. Eng. A*, vol. 639, pp. 647–655, 2015, doi: 10.1016/j.msea.2015.05.035.

[55] V. A. Popovich, E. V. Borisov, A. A. Popovich, V. S. Sufiiarov, D. V. Masaylo, and L. Alzina, “Impact of heat treatment on mechanical behaviour of Inconel 718 processed with tailored microstructure by selective laser melting,” *Mater. Des.*, vol. 131, no. May, pp. 12–22, 2017, doi: 10.1016/j.matdes.2017.05.065.

[56] D. Gu, Q. Shi, K. Lin, and L. Xi, “Microstructure and performance evolution and underlying thermal mechanisms of Ni-based parts fabricated by selective laser melting,” *Addit. Manuf.*, vol. 22, no. May, pp. 265–278, 2018, doi: 10.1016/j.addma.2018.05.019.

[57] Q. B. Nguyen, Z. Zhu, B. W. Chua, W. Zhou, J. Wei, and S. M. L. Nai, “Development of WC-Inconel composites using selective laser melting,” *Arch. Civ. Mech. Eng.*, vol. 18, no. 4, pp. 1410–1420, 2018, doi: 10.1016/j.acme.2018.05.001.

[58] L. Zhou, A. Mehta, B. McWilliams, K. Cho, and Y. Sohn, “Microstructure, precipitates and mechanical properties of powder bed fused inconel 718 before and after heat treatment,” *J. Mater. Sci. Technol.*, vol. 35, no. 6, pp. 1153–1164, 2019, doi: 10.1016/j.jmst.2018.12.006.

[59] B. Sutton, E. Herderick, R. Thodla, M. Ahlfors, and A. Ramirez, “Heat Treatment of Alloy 718 Made by Additive Manufacturing for Oil and Gas Applications,” *Jom*, vol. 71, no. 3, pp. 1134–1143, 2019, doi: 10.1007/s11837-018-03321-7.

[60] M. Pröbstle, S. Neumeier, J. Hopfenmüller, L. P. Freund, T. Niendorf, D. Schwarze, and M. Göken, “Superior creep strength of a nickel-based superalloy produced by selective laser melting,” *Mater. Sci. Eng. A*, vol. 674, pp. 299–307, 2016, doi: 10.1016/j.msea.2016.07.061.

[61] W. Tillmann, C. Schaak, J. Nellesen, M. Schaper, M. E. Aydinöz, and K. P. Hoyer, “Hot isostatic pressing of IN718 components manufactured by selective laser melting,” *Addit. Manuf.*, vol. 13, pp. 93–102, 2017, doi: 10.1016/j.addma.2016.11.006.

[62] W. M. Tucho and V. Hansen, “Characterization of SLM-fabricated Inconel 718 after solid solution and precipitation hardening heat treatments,” *J. Mater. Sci.*, vol. 54, no. 1, pp. 823–839, 2019, doi: 10.1007/s10853-018-2851-x.

[63] E. M. Fayed, D. Shahriari, M. Saadati, V. Brailovski, M. Jahazi, and M. Medraj, “Influence of homogenization and solution treatments time on the microstructure and hardness of Inconel 718 fabricated by laser powder bed fusion process,” *Materials (Basel).*, vol. 13, no. 11, 2020, doi: 10.3390/ma13112574.